



# Three-dimensional in situ observations of compressive damage mechanisms in syntactic foam using X-ray microcomputed tomography

M. E. Kartal<sup>1,2,\*</sup>, L. H. Dugdale<sup>1,2</sup>, J. J. Harrigan<sup>1,2</sup>, M. A. Siddiq<sup>2</sup>, D. Pokrajac<sup>2</sup>, and D. M. Mulvihill<sup>3</sup>

<sup>1</sup>Lloyd's Register Foundation Centre for Safety and Reliability Engineering, School of Engineering, University of Aberdeen, Aberdeen AB24 3UE, UK

<sup>2</sup>School of Engineering, University of Aberdeen, Aberdeen AB24 3UE, UK

<sup>3</sup>School of Engineering, University of Glasgow, James Watt South Building, Glasgow G12 8QQ, UK

Received: 5 April 2017

Accepted: 5 May 2017

Published online:

31 May 2017

© The Author(s) 2017. This article is an open access publication

## ABSTRACT

Syntactic foams with hollow glass microspheres embedded in an epoxy matrix are used in marine, aerospace and ground transportation vehicle applications. This work presents an in situ experimental study of failure mechanisms in syntactic foam based on X-ray microcomputed tomography with uniaxial compression. Under different levels of compressive strain, the material was scanned using X-ray microcomputed tomography to obtain three-dimensional (3D) images of its internal microstructure. Experiments with the same parameters were carried out to investigate repeatability. The microscopic observations have suggested that damage nucleation occurs at the weakest microspheres. When applied strain increases, shear collapse bands (SCBs) develop local to the fragmented microspheres due to stress concentration and bending deformation around SCBs occurs. After significant strain, the thickness of the SCBs increases owing to the accumulation of the broken microspheres. The relationship between the volume fraction of microspheres and applied bulk strain has been characterised.

## Introduction

Polymer matrix syntactic foams are low-density composite materials fabricated by randomly filling hollow particles into a material matrix. These foams are categorised as closed-cell foams because particles are not interconnected to each other and each pore is enclosed in the matrix. Hollow particles

have a significant effect on the properties of syntactic foams. Their microstructure is determined by the choice of particle materials, volume fraction and wall thickness of particles. Commonly used hollow particles in polymer matrix syntactic foams are glass, ceramic, carbon and fly ash cenospheres [1].

Hollow glass is one of the most commonly used particles, as they confer a variety of valuable

Address correspondence to E-mail: mehmet.kartal@abdn.ac.uk

properties such as low density, impact strength, thermal insulation, dimensional stability and low dielectric constant. In recent years, they are becoming more widely used as thermal insulation in the offshore oil extraction industry [1–4], being utilised in the subsea flowlines used to bring the oil from the extraction point up to the surface. As the earth's oil reserves are being depleted, there is an increased requirement to extract oil from harder to reach places, such as further out at sea and from greater depths (up to 3000 m). Extracting oil from these locations presents new challenges due to the low temperature and high pressure nature of deep sea water, as well as the increased cost of transportation to these more distant locations. The traditional pipe-in-pipe method of extraction is proving ineffective in these locations because of the extremely large weights of the pipes that are required. Constructing such heavy objects is demanding and costly and also requires larger vessels for transportation and installation. By using a single pipe with a glass bubble syntactic foam insulating layer, the overall weight of the flowline can be reduced by over fifty per cent whilst still maintaining the same level of thermal insulation, making extraction from these locations more feasible. The thermal insulation of the flowline is important as it is desirable to minimise heat lost from the oil to the sea water as much as possible. This is because the cooler the oil becomes, the greater the amount of energy required to pump it, resulting in an increased cost of the operation.

The syntactic foams are subjected to high pressure especially in deep water and must be durable in such harsh conditions as the deep sea environment. Therefore, a better understanding of the in-service failure mechanisms represents an important engineering challenge as a service-life of at least a couple of decades is envisaged.

Various different approaches have already been taken to understand macroscopic failure mechanisms in polymer/glass syntactic foams when subjected to different loading conditions [5–10]. It was found that crack directions (i.e. transverse, longitudinal and diagonal) dominantly depend on volume fraction and the geometry of particles.

As the global response of such materials is governed by their microstructures and deformation at the microscale level, understanding the 3D microstructural damage mechanisms of these materials under in-service conditions is key to

determining the limitations of such materials so that new stronger materials can be developed. Since syntactic foams possess complex and heterogeneous microstructures, their evaluations should be made in three dimensions. Although scanning electron microscopy (SEM) provides very high-resolution imaging, results are only limited to the free surface of a specimen. Recently, X-ray computed tomography has become an attractive characterisation technique in Materials Science as multiscale material behaviours can be obtained without sectioning specimens. With the very rapid growth of instrumentation over the last 15 years, it is now possible to obtain 3D images with a spatial resolution less than a micrometre by means of laboratory-based X-ray computed tomography.

Due to the above-mentioned traditional limitations, research on in situ damage characterisation of such materials in the literature is limited. Huang et al. [11] investigated the failure mechanism in cenosphere epoxy syntactic foams under quasi-static and dynamic loading. They found that, when compared to quasi-static loading, dynamic loading caused macro-cracks in the matrix to be formed at an earlier strain stage. Since their experimental set-ups were allowed to obtain 3D images with relatively low resolution (8  $\mu\text{m}$  voxel size), only syntactic foams with large glass sphere diameters could be monitored. Likewise, Balch et al. [12] investigated plasticity and damage in aluminium syntactic foams at quasi-static and dynamic strain rates. Microstructural features in deformed samples after the compression tests were observed with the help of tomographic images with 8.7  $\mu\text{m}$  voxel size.

Adrien et al. [3] conducted one of the first studies using X-ray microtomography to investigate internal microstructural damage in syntactic foams containing glass microspheres. They studied the compressive behaviour of three different matrix materials (i.e. polypropylene, polyurethane and an epoxy resin) using high-resolution synchrotron X-ray microtomography. By processing 3D images obtained at both initial and compressed states, the morphology of microspheres was analysed for the three different materials. With the help of synchrotron radiation, very high-resolution images with 0.7  $\mu\text{m}$  pixel size were obtained. The results showed that when the matrix material was soft as is the case for polypropylene and polyurethane, the foam was able to deform significantly under compression and as

such, the load was spread equally among all of the spheres. This uniform loading distribution, combined with the fact that all the spheres had the same wall thickness, meant that the fracture of spheres was dependent only on their radius. It was observed that the spheres with a larger radius ruptured earlier than the spheres with a smaller radius. In the case of the epoxy resin, which has a relatively higher Young's Modulus, the matrix deformed less under compression and so the load was not able to be spread equally among the microspheres. The result of this was that fracture of the spheres was dependent on their location rather than their radius.

In the experimental studies mentioned above [3, 11, 12], the scans were not recorded during one single experiment. After each stage of compression, the specimens were unloaded and placed into the X-ray machine for a new scan.

In the work of Lachambre et al. [13], the hydrostatic compression behaviour of syntactic polymer foams (polypropylene and polyurethane) with and without hollow glass microspheres was studied with the help of high-resolution X-ray tomography. The specimens were submerged in ethanol, and local damage incidences, swelling of the matrix and the morphology of filled-in spheres were compared between three different materials under in situ compressive loading.

A closer examination of the failure mechanism of polymer matrix syntactic foams reinforced with cenospheres subjected to compression is provided by Huang et al. [14]. Here, it was observed that the failure of syntactic foams was due to both crushing of the glass spheres and plastic deformation of the matrix. They noted that the damage bands occurred preferentially along the diagonal of the specimen. They also found that the largest spheres fractured before the smaller ones and the fracture takes place in the external compressive loading direction. This investigation was conducted on glass spheres with very large external diameters ranging from 200 to 600  $\mu\text{m}$ . As with their prior investigation [11], this analysis was done on syntactic foam using low-resolution tomography and hence this experimental set-up would not permit investigation of syntactic foams with small sphere diameters. Thus, only basic information could be obtained from the images produced and, hence, there is a need to investigate the failure behaviour more closely using higher resolution. In addition, as a load cell was not integrated into the loading stage, the loads being applied to the

specimen were not known and hence the scans were taken at chosen strain values instead of at significant points in the stress–strain curve such as the compressive strength and sequentially along the curve in the plateau region. Another limitation is that the strain values between two subsequent images were large and damage nucleation was not captured.

The aim of this study is to investigate damage mechanisms of syntactic foam under uniaxial compressive load. Images at different stages of deformation were obtained by the combined use of high-resolution X-ray microcomputed tomography with an in situ tension/compression testing stage allowing observations of 3D deformation. By repeating the test under the same experimental parameters, the repeatability of the results has been investigated. In order to better understand damage nucleation, a higher scanning frequency was used for the early stage of damage accumulation.

## Material and specimens

The material used in this investigation was syntactic foam provided by Trelleborg. This consisted of hollow glass spheres embedded within an epoxy matrix. This material has recently been found to be useful in the offshore oil extraction industry, as a replacement for traditional pipe-in-pipe method of extraction, being utilised in the subsea flowlines used to bring the oil from the extraction point up to the surface.

The glass spheres are added to the polymer as it is being extruded whilst it is in its liquid state. The epoxy matrix was made through a batch mixing process with a post-cure (anhydride catalyst). The glass spheres used adhered to the company's K25 specifications [15], given in Table 1.

Prismatic blocks were machined from a bar with the dimensions  $10 \times 10 \times 10 \text{ mm}^3$ . Then the surfaces of the specimen were ground using abrasive paper to produce flat surfaces and reduce the stress concentrations experienced when placed in the testing apparatus.

## Experimental procedures

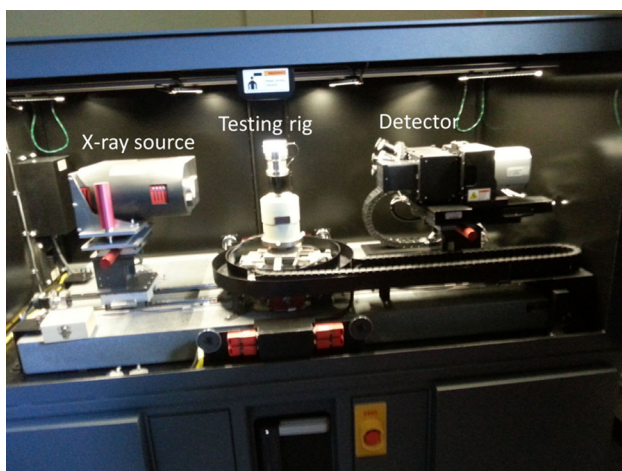
X-ray microcomputed tomography was conducted using the laboratory-based ZEISS VersaXRM-410 machine, which has a minimum spatial resolution of

**Table 1** Glass sphere properties provided by the manufacturer [15]

Particle size ( $\mu\text{m}$ , volume)			Effective top size ( $\mu\text{m}$ )	True density (g/cc)	Target crush strength (90% survival, psi)
Distribution					
10th%	50th%	90th%			
25	55	90	105	0.25	750

0.9  $\mu\text{m}$ , minimum voxel size of 0.1  $\mu\text{m}$ , a maximum power output and voltage of 10 W and 150 kV, respectively, [16]. The term spatial resolution represents important features of the system including spot size, resolution of the detector and magnification geometry. A microtension/compression testing stage with a  $\pm 5\text{kN}$  capacity load cell (Deben, UK) was mounted on the stage of the X-ray machine. Figure 1 shows the experimental configuration indicating key features such as the X-ray source, detector and tension/compression testing rig. The sample was loaded into the Deben rig at a central position in a 3-mm thick vitreous glassy carbon tube providing low X-ray attenuation. The dimensions of the specimen were specially chosen such that the load required to reach beyond the elastic limit would not exceed the capacity of the load cell and also to ensure adequate X-ray transmission to get high-resolution radiographs.

The specimens being tested were subjected to unconstrained, uniaxial, quasi-static compression and scanned at various different levels of strain. Figure 2 depicts a schematic of the view of the

**Figure 1** Photograph of apparatus in situ, showing X-ray source, detector and tension/compression rig.

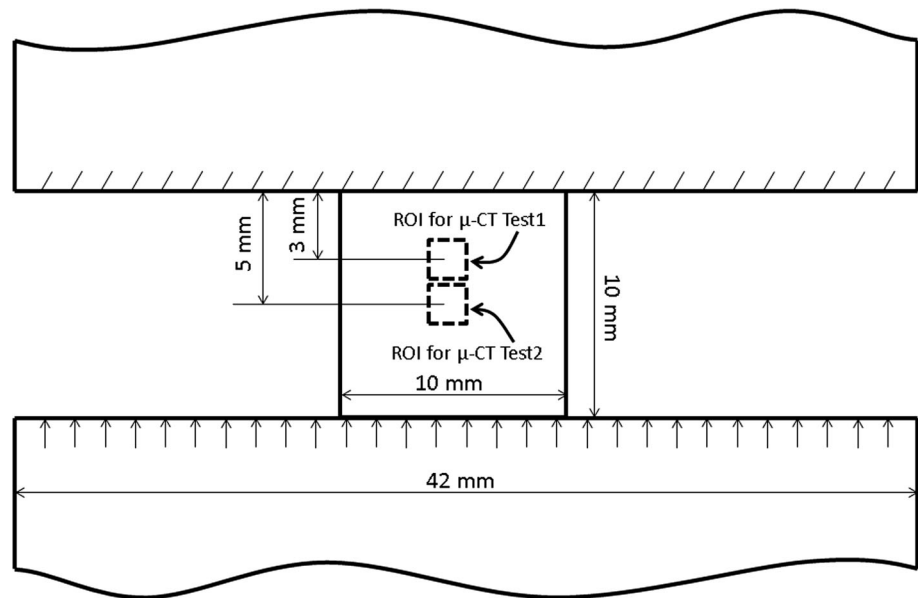
compressive loading. The top and bottom surfaces of the specimen were placed in the grips of the testing machine. The top grip remained stationary, whilst the bottom grip moved upwards to compress the specimen. The compressive load was applied to the specimen under the displacement control mode at ambient temperature. The strain was held constant at the target value during each scan before being increased up to the level at which the next scan was taken. Applied load and displacement are controlled and recorded using stage control software giving a range of control functions.

Two specimens were scanned under uniaxial compressive tests. Since time and cost involved were high and the repeatability was found to be good in two sets of experiments, we did not perform further experiments. The first specimen was scanned at 13 different deformation stages, and nominal strains of 37% were reached in compressive tests. The second specimen was scanned at 9 different levels of compression until a strain value reached 18%. The specimen was compressed at a rate of 0.1 mm/min

For each specimen, the first scan was taken of the material when it was under a very small load to show it in its undeformed configuration, followed by a scan at a strain value of 4% as this was predicted to be within the linear elastic region. In order to observe the early stage of damage accumulation, several scans were taken shortly after the specimen was observed to reach its elastic limit and began deforming plastically.

Each scan was run at an X-ray beam energy of 140 kV and a power of 10 W. The distance between the specimen and X-ray source was 84 mm while there was 244 mm between the specimen and detector. An optical magnification of  $4\times$  was used to achieve high resolution. This gave a 1.7- $\mu\text{m}$  pixel size for  $1024 \times 1024$  pixel projection images. Exposure time was set to 20 s in order to get intensity values being 5000 or above for the best signal-to-noise ratio

**Figure 2** Schematic diagram of specimen showing applied loads, key dimensions and positions of regions of interest in which tomographic images are obtained under compressive loadings.



for each projection (radiograph). Sets of 2400 and 3200 projections were captured over 360° of sample rotation for the first and second specimens, respectively. Figure 2 shows the locations where the tomographic images were acquired. In order to reduce a rigid body motion due to large strain being applied to the first specimen, the centre of the region of interest (ROI) in the first specimen was chosen to be 7 mm away from the bottom surface of the specimen in the z-direction and to be in the centre of the XY plane, whereas the centre of the ROI was in the centre of the second specimen.

The 2D radiographs were reconstructed into 3D images using the Xradia XMReconstructor software. Beam hardening and centre shift artefacts were removed as part of the reconstructing process. Post-processing analysis of the data obtained was possible using Avizo computer software.

## Results and discussion

Using Deben stage control software, the stress–strain data obtained from both tests were recorded. For comparison, a compression test on another specimen with the same dimensions was performed at a displacement rate of 0.1 mm/min while no images were recorded to interrupt the test. Figure 3 shows a comparison of the stress–strain curves obtained from compression tests. Three curves are shown: those labelled ‘μ-CT Test1’ and ‘μ-CT Test2’ were obtained from the samples when the X-ray was turned on and

the radiographs were taken by means of holding the compressive strain constant, while the curve labelled ‘Single compression test without holding the load’ is based on a continuous compression test without holding strain at any stage of the test. Note that nominal stress versus engineering strain is used in Fig. 3.

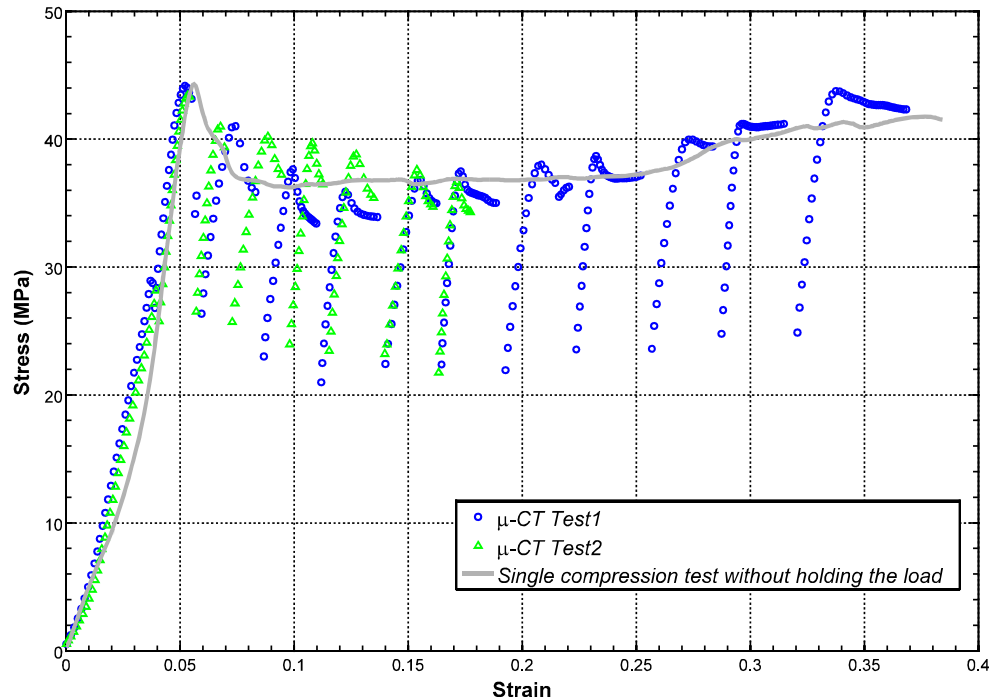
As can be seen from the continuous compression test in Fig. 3, the syntactic foam undergoes three different states of deformation: (1) the initial elastic region in which almost linear relationship between stress and strain is observed (2) a plateau regime where stress varies in a small range after reaching its maximum value and a sudden drop in stress, and (3) a densification regime characterised by an increase in stress.

In the first region, the deformation state is uniform in the syntactic foam until the stress value reaches compressive (peak) strength. The peak strength was found to be about 43 MPa. After the stress reaches its peak value, there is a decrease in stress by at least 10%. This decrease corresponds to the initiation of microsphere crushing. The plateau region in the second stage of the stress–strain curve occurs due to crushing of microspheres and hence the exposing of the internal hollow volume which is filled by fragmented glass spheres and foam.

The reason for this fluctuation in stress is caused by the relative strength mismatch between particle and foam [1]. When the strain value reaches about 20–25%, the stress begins to increase owing to densification.



**Figure 3** Compressive stress–strain curves of the syntactic foam specimens with and without  $\mu$ -CT scanning.



The sudden drops in stress for a given value of strain in the curves labelled  $\mu$ -CT Test1' and ' $\mu$ -CT Test2' in Fig. 3 represent the parts of the test where the strain was held constant while an X-ray tomographic scan of the specimen was conducted. When the material is held at a constant strain over a period of time, stress relaxation of the specimen occurs due to energy dissipation and this results in a decreased amount of stress necessary to maintain the same amount of strain. This is emphasised by the fact that when the specimen is scanned whilst it is still in the linear elastic region, there is no significant stress relaxation. Given that it took approximately 18 h to perform one scan of the specimen, it was possible that stress relaxation could occur whilst the scan was taking place, changing the internal structure of the material and thus distorting the image obtained. To account for this, the specimen was left at a constant level of strain for a period of 1 h before each scan was started, thus minimising any negative impact on the quality of the images produced. The graph shows that, even though the strain is increased between every scan, the applied stress needed to cause these strains does not vary much between consecutive scans due to stress relaxation.

For the first sample ( $\mu$ -CT Test1), we observed the microstructures and damage accumulation under 13

different engineering compressive strains. In order to fit the images on the paper, 12 of them will be presented here obtained under the strain values of 0.0,  $-4.2$ ,  $-5.8$ ,  $-8.6$ ,  $-11.1$ ,  $-13.7$ ,  $-16.3$ ,  $-19.0$ ,  $-22.1$ ,  $-28.4$ ,  $-31.6$  and  $-36.8\%$ . Three-dimensional cut-outs of the larger image were produced, and these are shown in Fig. 4. All of the cut-outs taken were of the same dimensions ( $0.5 \text{ mm} \times 0.5 \text{ mm} \times 1 \text{ mm}$ ). All of the images are given to the same scale and from the same viewing angle. Note that the features highlighted in green in Fig. 4 show the locations of the vertices and centres of the edges.

Figure 5 shows the XZ planes of the 3D images produced from the X-ray computed tomography at 12 different levels of strain in the first sample ( $\mu$ -CT Test1). As the compression increased, it was observed that there was some movement of individual glass spheres relative to each other in the lateral direction. For this reason, the cross sections at each level of strain are taken from slightly different locations so that the same portion of material is being shown in each image. For the first cross section, a location was chosen approximately in the middle of the image, where a distinct feature could be observed. All subsequent cross sections were chosen so that the same feature can be observed in the rest of the images. All of the images are given to the same scale ( $1.74 \text{ mm}$  by

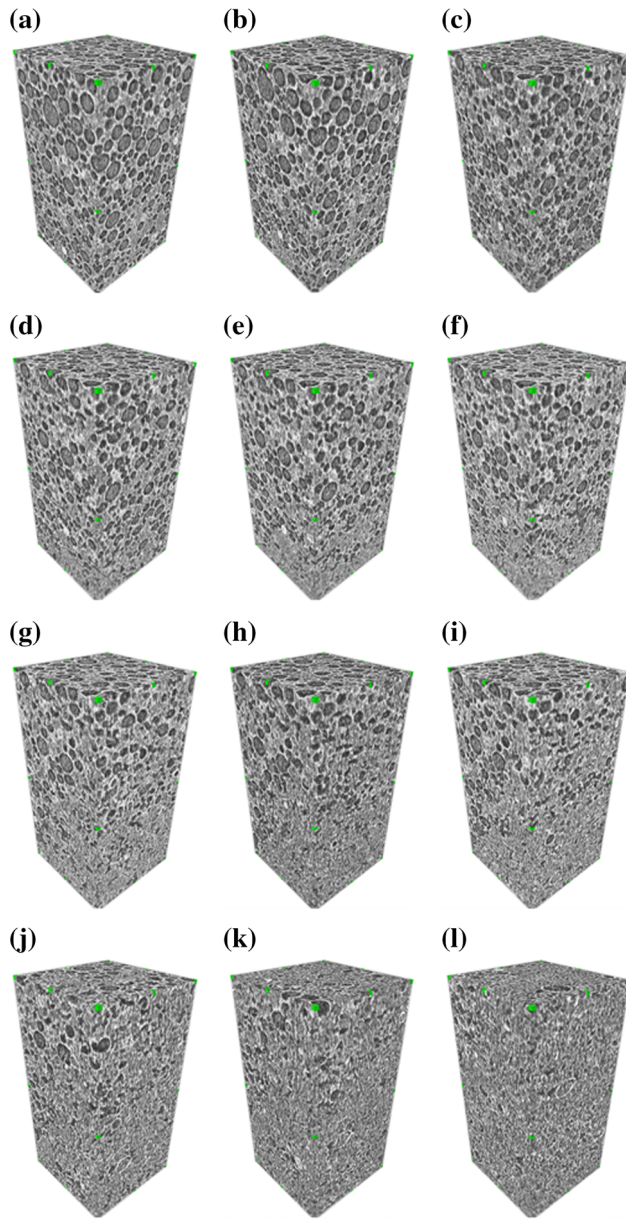


**Figure 4** 3D observations of internal microstructure and failure process of the syntactic foam obtained from  $\mu$ -CT Test1 at strains **a** 0.0, **b**  $-4.2\%$ , **c**  $-5.8\%$ , **d**  $-8.6\%$ , **e**  $-11.1\%$ , **f**  $-13.7\%$ , **g**  $-16.3\%$ , **h**  $-19.0\%$ , **i**  $-22.1\%$ , **j**  $-28.4\%$ , **k**  $-31.6\%$  and **l**  $-36.8\%$ .

1.74 mm), with the load being applied in the vertical upward direction.

Figures 4a and 5a show the natural state of the syntactic foam under the very light load (i.e.  $-10$  N). In Figs. 4b and 5b, deformation is elastic and the syntactic foam is observed to move in the vertical upward direction without observing any damage or failure of microspheres. The subsequent image was

taken shortly after the specimen was observed to reach its compressive strength during the compression test (Figs. 4c, 5c). Here, damage has already initiated with several microspheres already fragmented especially at the bottom of the ROI. In addition, a shear collapse band (SCB) developed local to the fragmented microspheres due to stress concentration as highlighted in Fig. 5c. As expected from syntactic foams with high volume fraction of microspheres, slip bands evolve diagonally. When the compressive strain reached the value of  $-8.6\%$  in Fig. 5d, the movement of the particles in the vertical direction is not observed but a bending deformation mechanism around the SCB band is observed.

In Fig. 5e, there are two more thickened SCBs developed and they met each other as shown with the light lines. In Fig. 5f, as the two shear bands interacted each other, the direction of the SCB at the bottom of the right-hand side of the image changed and almost combined with the other SCB at the bottom of the left-hand side of the image. During this damage process, crushed microspheres were piled up in this region. Note that this deformation mechanism is also observed in metallic foams [17].

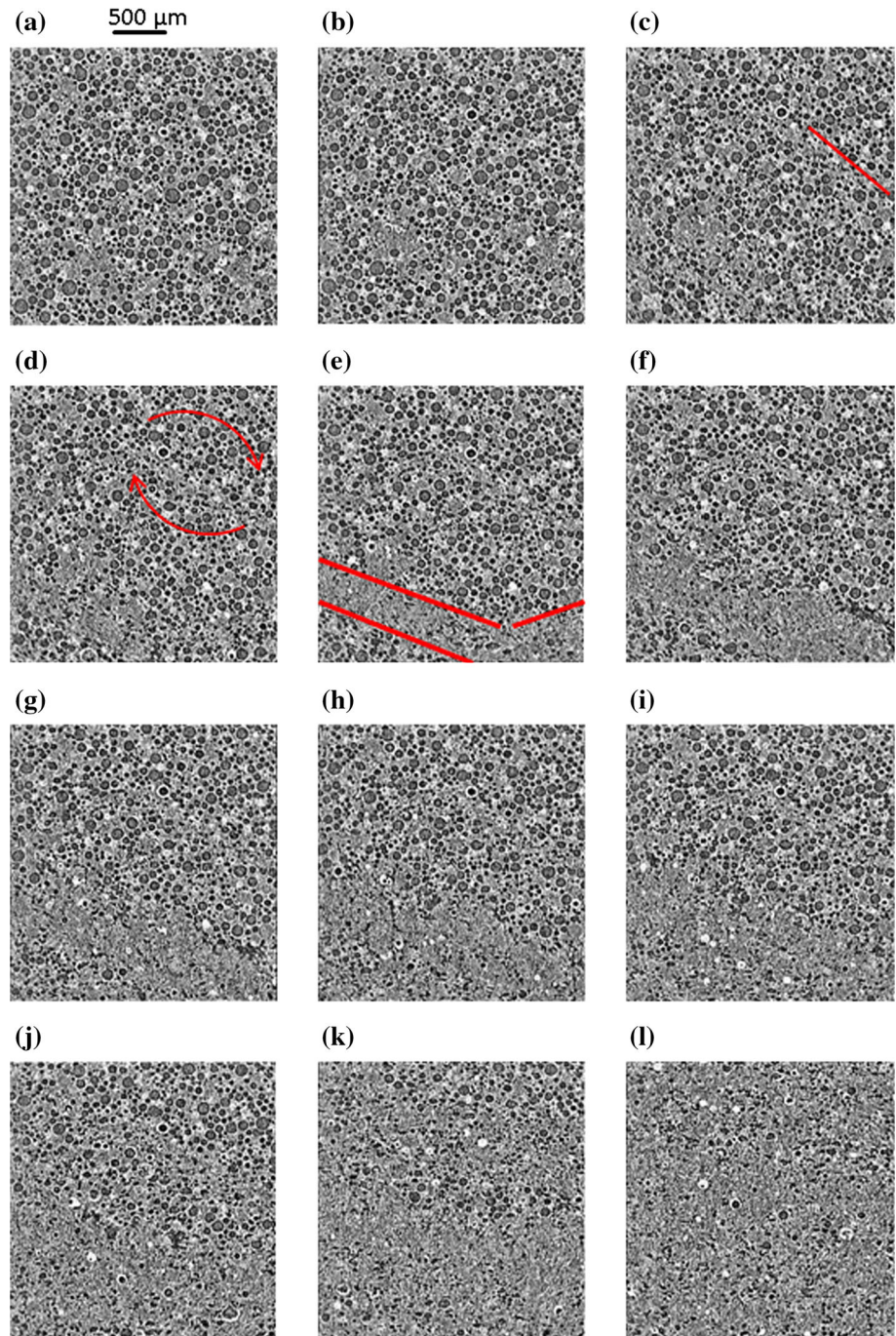
It can be seen from the subsequent images that the crushed microspheres and thickness of the SCBs increase with increased compression in the plateau regime. When the strain value reached  $-36.8\%$ , most microspheres were fragmented and compressed.

Figure 6 shows deformation mechanisms at the XZ planes of 3D tomographic images obtained from the scans within the second specimen ( $\mu$ -CT Test2) under nine different engineering strains: (a) 0, (b)  $-4.0\%$ , (c)  $-5.5\%$ , (d)  $-7.1\%$ , (e)  $-9.7\%$ , (f)  $-11.4\%$ , (g)  $-13.8\%$ , (h)  $-16.3\%$ , and (i)  $-17.8\%$ . The 2D images presented were extracted parallel to the loading axis (vertical in the figure) and approximately at the centre of the  $y$ -direction. Once again, the 2D planes at each level of strain were extracted from slightly different locations so that the same region of material is shown for each image. Each image is given to the same scale (1.74 mm by 1.74 mm).

Figure 6a shows the microstructure of the syntactic foam prior to deformation, and there is no pre-broken glass microspheres observed. Figure 6b displays an initial linear elastic region in which the region of interest moves in the vertical direction without any damage to the microspheres. After the first (elastic) stage of compression (Fig. 6c), a few broken microspheres at the top of the image are observed. At the



**Figure 5** XZ images extracted from the 3D images showing internal microstructure and failure process of the syntactic foam obtained from  $\mu$ -CT Test1 at different strains **a** 0.0, **b**  $-4.2\%$ , **c**  $-5.8\%$ , **d**  $-8.6\%$ , **e**  $-11.1\%$ , **f**  $-13.7\%$ , **g**  $-16.3\%$ , **h**  $-19.0\%$ , **i**  $-22.1\%$ , **j**  $-28.4\%$ , **k**  $-31.6\%$  and **l**  $-36.8\%$ .



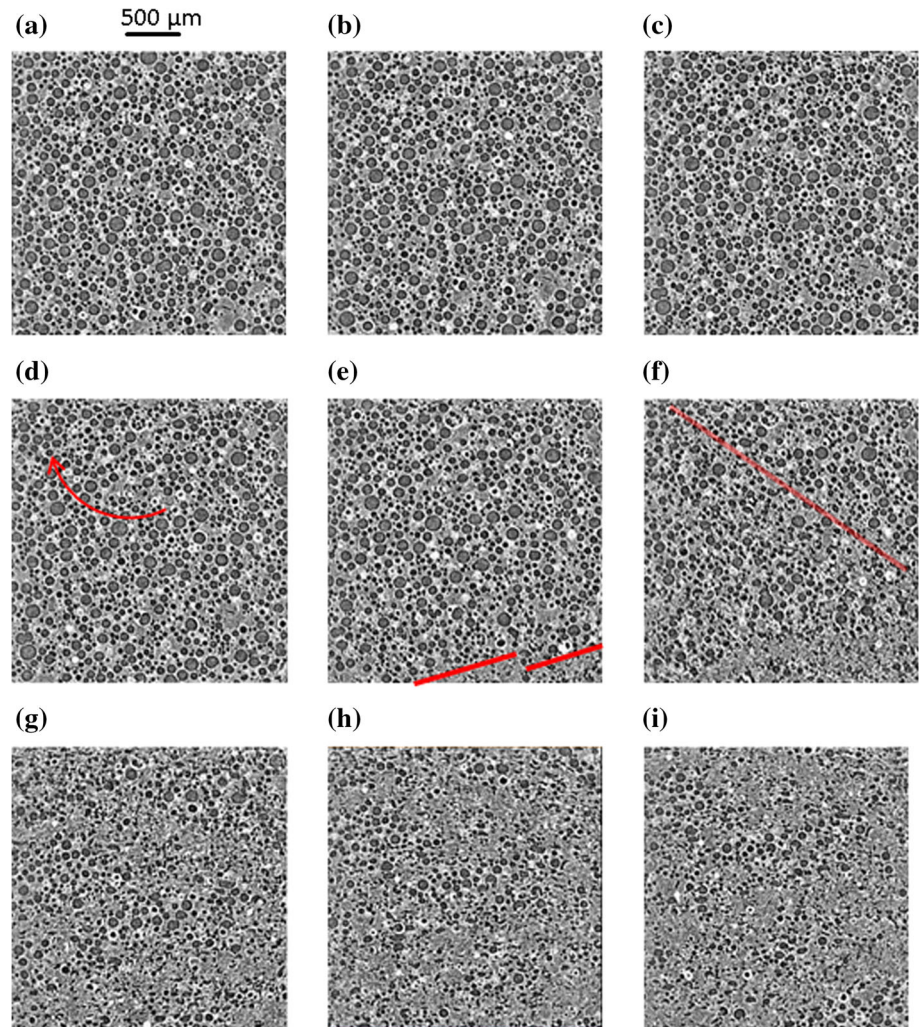
increased strain (Fig. 6d), a whole region of interest around the broken microspheres was undergoing bending without any further breakage of the microspheres.

When the strain value reached  $-9.7\%$ , two distinguished SCBs along the diagonal of the specimen due to the crushing of microspheres are observed as highlighted in red on the image in Fig. 6e. In the

following image (in Fig. 6f), these two SCBs were thickened and an additional SCB in the central part emerged. At the strain value of  $-13.8\%$  (Fig. 6g), many of the microspheres are crushed and the thickness of the existing SCBs increases. The subsequent damage accumulation in the form of collapsed/fragmented particles progresses with an increase in compressive strain in Fig. 6h, i.



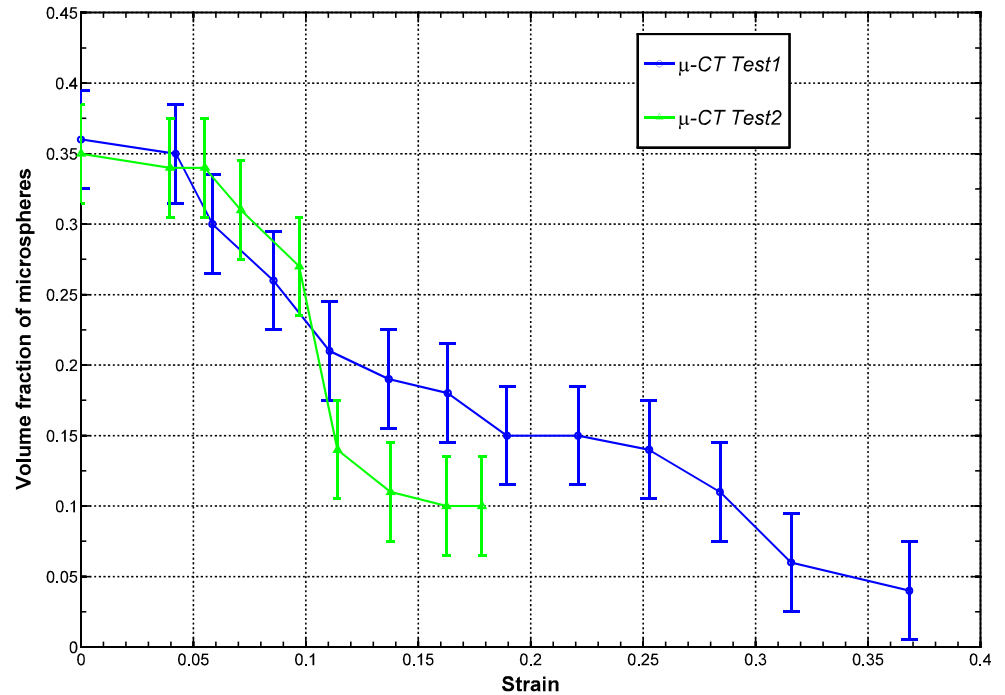
**Figure 6** XZ images extracted from the 3D images showing internal microstructure and failure process of the syntactic foam obtained from  $\mu$ -CT Test2 at different strains **a** 0, **b**  $-4.0\%$ , **c**  $-5.5\%$ , **d**  $-7.1\%$ , **e**  $-9.7\%$ , **f**  $-11.4\%$ , **g**  $-13.8\%$ , **h**  $-16.3\%$ , and **i**  $-17.8\%$ .



Segmentation was performed in order to differentiate between the matrix material and the glass microspheres. In this way, the segmented images allowed for a volume fraction analysis to be performed. The volume fraction of glass spheres at each of the strain levels for each set of experiments was calculated. It should be noted that since the field of view chosen for  $\mu$ -CT tests is very small (1.74 mm in length), microspheres observed at the top side of the frame at the natural state of the syntactic foam move out of the frame as the strain is increased and new microspheres at the bottom side of the imaging frame will appear. In addition, there are variations in volume fraction of the microsphere (up to 3.5%) at different planes noted. Uncertainties in the volume fraction calculations therefore have an effect, and it is not an easy task to evaluate the volume fraction with a very high degree of accuracy. They were hence taken as an indication of the uncertainty in the

calculation of volume fraction. Figure 7 shows the variation of the calculated volume fraction of the microspheres as a function of the strain applied for each of the  $\mu$ -CT tests. The nominal volume fraction of the spheres at the natural state was determined to be around 0.36. As expected, the volume fraction of microspheres decreases when the strain is increased. This is a result of the spheres fracturing due to the applied load, with more spheres fracturing as the load is increased. Error bars are denoted, but it is seen that the variation is smooth, suggesting that the uncertainty is lower than that assumed. As can be seen from the figure, the agreement between two sets of experiments is very close until the  $-10\%$  strain value is reached. Due to crushing of many microspheres in the second specimen at the strain value of  $-11.4\%$ , the difference in volume fraction between two different experiments becomes more pronounced.

**Figure 7** Volume fraction of spheres versus compressive strain.



As can be observed in Figs. 5 and 6, some microspheres change their shapes considerably before finally fracturing. In order to examine this more closely, 3D images of a set of four individual glass microspheres were created and tracked during deformation (using the 3D field labelling function in Avizo). The images (Fig. 8) show the microspheres moving towards each other and then contacting and becoming oblate spheroid before finally fracturing in smaller fragments. Note that this mechanism has been also observed in elsewhere [14, 18]. The dimensions of the particles at each stage are given in Table 2. This figure indicates that particle interaction and coalescence also form a critical element of the damage process, as well as, the individual collapse of independent particles.

As can be seen from two different sets of experiments (Figs. 3, 4, 5, 6), there are several failure mechanisms developed during the compressive loading in syntactic foam. The first failure initiation is due to crushing of microspheres just after the applied load reaches the compressive strength. The breakage of the individual microsphere causes the load to transfer to neighbouring microspheres. Due to a stress concentration around the broken microsphere, adjacent microspheres are also broken and the formation of localised SCBs due to collapsed/fragmented microspheres evolves diagonally to the

loading direction. This failure mechanism is generally found in syntactic foams with high volume fraction of microspheres [14]. The exposed internal hollow volume of broken microspheres is filled by fragmented glass spheres and foam. Owing to accumulation of the broken microspheres and stress concentrations, the thickness of the SCB increases when the applied strain is increased in the plateau region. Furthermore, a bending deformation around the SCB is observed. Later, an accumulation of random shear collapse bands appears, and these shear collapse bands meet and interact. This process can cause the change in orientations of the SCBs. A feature of slight plastic hardening in the plateau region of the stress–strain curves may be attributed to this effect. Once nearly all microspheres are broken, there will be no more empty volume to be exposed and filled by the foam matrix, and further compression results in a densification region.

The comparison of the microstructural changes of the syntactic foam obtained from two different sets of experiments during compressive tests shows that SCBs develop at different random locations in the specimen. This can be explained by the phenomenon that relatively weak spheres are first crushed and then induce the damage of surrounding microspheres to form SCBs due to minimal energy-consumption. Therefore, the quasi-static initial failure

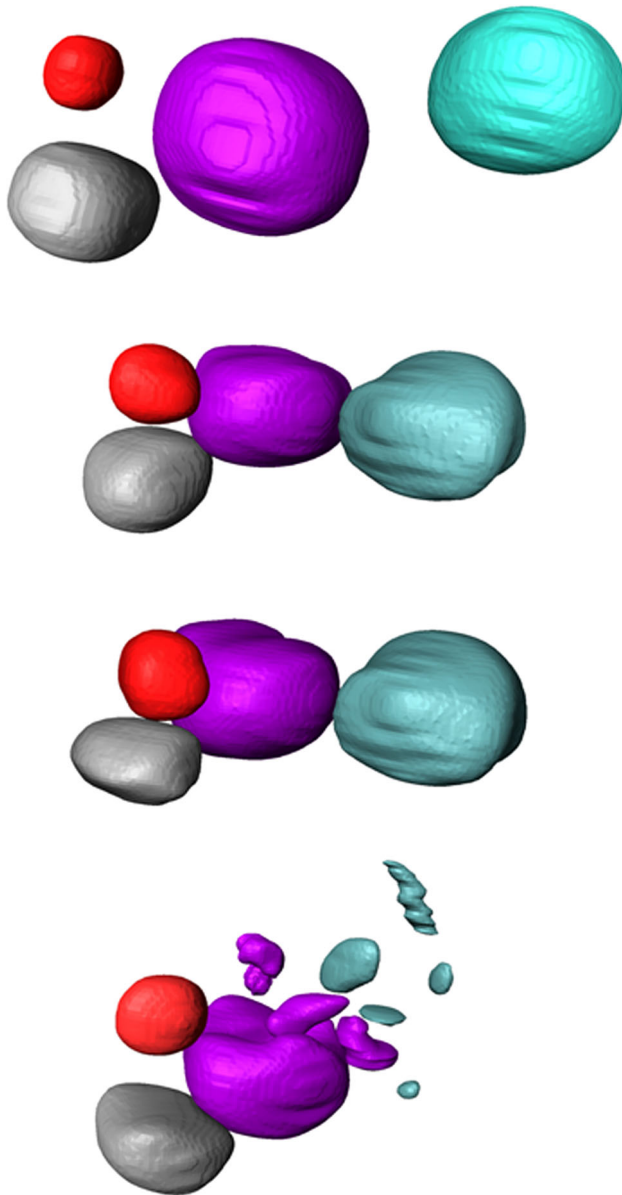


**Figure 8** Evolution of glass particle position and shape during foam compression with eventual particle coalescence and fracture (for set of four representative particles).

stress depends on the strength of the weakest microspheres. Failure mechanisms might be different at and near to unsupported exteriors due to the effect of free-traction boundary conditions. However, examining failure mechanisms away from free surfaces are more representative when considered under in-service loading conditions.

## Conclusion

The paper presents an experimental study of failure processes in hollow glass microsphere/epoxy-based syntactic foam under compressive loading. In situ compression testing was carried out with X-ray microcomputed tomography allowing full-field, high-resolution 3D observation of deformation. Two sets of experiments with the same experimental parameters were conducted to assess repeatability. The results suggest that failure initiates at weak microspheres and propagates from these locations. A number of concurrent failure mechanisms occur during the plateau phase of the foam stress–strain curve, including: crushing of individual microspheres, formation of shear collapse bands (SCBs) diagonal to the loading direction, accompanying bending deformation and subsequent thickening of the SCBs as regions of fragmented microspheres expand. Microsphere interaction also forms a critical part of the damage process with initially separated microspheres coalescing under deformation in addition to breakage of independent microspheres.

## Acknowledgements

This work was financially supported by the Lloyd's Register Foundation Centre, the Royal Society (RG140680), and Oil and Gas Academy of Scotland.

**Table 2** Individual particle dimensions at different levels of strain obtained from  $\mu$ -CT Test2

Strain%	Green particle length		Purple particle length		White particle length		Red particle length	
	Horizontal	Vertical	Horizontal	Vertical	Horizontal	Vertical	Horizontal	Vertical
5.5	70	70	90	90	55	55	40	40
13.8	60	70	95	60	60	50	35	40
16.3	60	70	95	55	60	40	30	40
17.8	NA	NA	95	45	60	35	40	40



**Open Access** This article is distributed under the terms of the Creative Commons Attribution 4.0 International License (<http://creativecommons.org/licenses/by/4.0/>), which permits unrestricted use, distribution, and reproduction in any medium, provided you give appropriate credit to the original author(s) and the source, provide a link to the Creative Commons license, and indicate if changes were made.

**Electronic supplementary material:** The online version of this article (doi:[10.1007/s10853-017-1177-4](https://doi.org/10.1007/s10853-017-1177-4)) contains supplementary material, which is available to authorized users.

## References

- [1] Pinisetty D, Shunmugasamy VC, Gupta N (2015) Hollow glass microspheres in thermosets—epoxy syntactic foams. In: Amos SE, Yalcin B (eds) *Hollow glass microspheres for plastics, elastomers, and adhesives compounds*. Elsevier, Amsterdam, pp 147–174
- [2] Bardella L, Genna F (2001) On the elastic behavior of syntactic foams. *Int J Solids Struct* 38(40–41):7235–7260
- [3] Adrien J, Maire E, Gimenez N, Sauvart-Moynot V (2007) Experimental study of the compression behaviour of syntactic foams by in situ X-ray tomography. *Acta Mater* 55:1667–1679
- [4] Gupta N, Zeltmann SE, Shunmugasamy VC, Pinisetty D (2013) Applications of polymer matrix syntactic foams. *J Miner Metals Mater Soc* 66(2):245–254
- [5] Gupta N, Woldesenbet E, Mensah P (2004) Compression properties of syntactic foams: effect of cenosphere radius ratio and specimen aspect ratio. *Compos A Appl Sci Manuf* 35:103–111
- [6] Kim HS, Plubrai P (2004) Manufacturing and failure mechanisms of syntactic foam under compression. *Compos A Appl Sci Manuf* 35(9):1009–1015
- [7] Wouterson EM, Boey FYC, Hu X, Wong S-C (2005) Specific properties and fracture toughness of syntactic foam: effect of foam microstructures. *Compos Sci Technol* 65(11–12):1840–1850
- [8] Li P, Petrinic N, Siviour CR, Froud R, Reed JM (2009) Strain rate dependent compressive properties of glass microballoon epoxy syntactic foams. *Mater Sci Eng A* 515(1–2):19–25
- [9] Pellegrino A, Tagarielli VL, Gerlach R, Petrinic N (2015) The mechanical response of a syntactic polyurethane foam at low and high rates of strain. *Int J Impact Eng* 75:214–221
- [10] Swetha C, Kumar R (2011) Quasi-static uni-axial compression behaviour of hollow glass microspheres/epoxy based syntactic foams. *Mater Des* 32(8–9):4152–4163
- [11] Huang R, Li P, Wang Z, Liu T (2016) X-ray microtomographic characterization and quantification of the strain rate dependent failure mechanism in cenosphere epoxy syntactic foams. *Adv Eng Mater*. doi:[10.1002/adem.201600215](https://doi.org/10.1002/adem.201600215)
- [12] Balch DK, O'Dwyer JG, Davis GR, Cady CM, Gray GT, Dunand DC (2005) Plasticity and damage in aluminum syntactic foams deformed under dynamic and quasi-static conditions. *Mater Sci Eng A* 391(1–2):408–417
- [13] Lachambre J, Maire E, Adrien J, Choqueuse D (2013) In situ observation of syntactic foams under hydrostatic pressure using X-ray tomography. *Acta Mater* 61:4035–4043
- [14] Huang R, Li P, Liu T (2016) X-ray microtomography and finite element modelling of compressive failure mechanism in cenosphere epoxy syntactic foams. *Compos Struct* 140:157–165
- [15] M: Product information. 3M™ Glass Bubbles, K Series, S Series. Energy and advanced [www.3M.com/microspheres](http://www.3M.com/microspheres)
- [16] Xradia, Inc Product overview. VersaXRM-410. <http://www.xradia.com/>
- [17] Zheng Z, Wang C, Yu J, Reid SR, Harrigan JJ (2014) Dynamic stress–strain states for metal foams using a 3D cellular model. *J Mech Phys Solids* 72(1):93–114
- [18] Zhang Q, Lee PD, Singh R, Wu G, Lindley TC (2009) Micro-CT characterization of structural features and deformation behavior of fly ash/aluminum syntactic foam. *Acta Mater* 57:3003–3011